

# Covering factors of the dusty obscurers in radio-loud and radio-quiet quasars

Maitrayee Gupta<sup>★</sup>, Marek Sikora<sup>†</sup>, Krzysztof Nalewajko<sup>‡</sup>

*Nicolaus Copernicus Astronomical Center, Bartycka 18, 00-716 Warsaw, Poland*

Last updated 2016 March 11; in original form 2016 March 11

## ABSTRACT

We compare covering factors of circumnuclear dusty obscurers in radio-loud and radio-quiet quasars. The radio-loud quasars are represented by a sample of FR II quasars obtained by cross-matching a catalog of the FR II radio sources selected by van Velzen et al. with the SDSS DR7 catalog of quasars. Covering factors of FR II quasars are compared with covering factors of the radio-quiet quasars matched with them in redshift, black hole mass, and Eddington-ratio. We found that covering factors, proxied by the infrared-to-bolometric luminosity ratio, are on average slightly smaller in FR II quasars than in radio-quiet quasars. For both samples, no statistically significant dependence of a median covering factor on Eddington ratio, black hole mass, nor redshift can be claimed.

**Key words:** quasars: general – infrared: galaxies

## 1 INTRODUCTION

Discovery of broad lines and strong non-stellar continuum in polarized light of Seyfert 2 galaxies (Antonucci & Miller 1985; Miller & Goodrich 1987) and thermal IR excesses (Miley et al. 1985; Edelson et al. 1987) led to idea about existence in AGN of dusty, molecular tori (Krolik & Begelman 1988). This allowed to unify Seyfert 2 galaxies (only narrow lines and weak or absent non-stellar continuum) with Seyfert 1 galaxies (broad emission lines and strong non-stellar continuum). The dusty tori were proposed also to unify narrow-line radio galaxies with radio-loud (RL) quasars and broad-line radio galaxies (Barthel 1989), and discovery of radio-quiet (RQ) quasars of type 2 (Reyes et al. 2008 and refs. therein) confirmed the presence of dusty obscurers in RQ quasars as well.

As indicated by the number ratio of the type 2 AGN to the type 1 AGN, and, independently, by the infrared-to-UV luminosity ratio, these tori are geometrically thick. They are predicted to have inner edge at the sublimation radius (Rees et al. 1969; Barvainis 1987) and are likely enclosed within the BH influence sphere (Hopkins et al. 2012 and refs. therein). Location of the inner edge at the sublimation radius is confirmed by reverberation mappings (e.g. Koshida et al. 2014) and by near-IR interferometry (Kishimoto et al. 2012), while constraints on their spatial extensions are suggested by the mid-IR interferometry (Burtscher et al. 2013; López-Gonzaga et al. 2016). Hence, studies of such tori provide excellent opportunity to probe the conditions of the outermost portions of the BH accretion flows. Unfortunately, physical

and dynamical structure of dusty tori is still not known (see review by Netzer 2015). It is even uncertain, whether they are really tori, or maybe they are just mimicked by optically thick portions of disk winds (e.g. Emmering et al. 1992; Königl & Kartje 1994; Elitzur & Shlosman 2006) or by warped, tilted accretion disks (Lawrence & Elvis 2010 and refs. therein). One might try to resolve the real structure of the dusty region by modeling spectra of IR radiation resulting from reprocessing of optical/UV central radiation. However, due to the complexity of these models, the observed spectra can be reproduced by many of them with a broad choice of the adopted model parameters (Netzer et al. 2015).

Regardless of the uncertainties in the ‘torus’ structure, using the mid-IR spectra one can at least study the fraction of the central radiation that is reprocessed by circumnuclear dust ( $R \equiv L_{\text{MIR}}/L_{\text{bol}}$ ), in particular its distribution and dependence on the Eddington ratio ( $\lambda_{\text{E}} \equiv L_{\text{bol}}/L_{\text{Edd}}$ ) and black hole mass ( $M_{\text{BH}}$ ). Noting that luminous RQ and RL quasars cover similar ranges of these parameters, by comparing above properties in these two quasar populations one may try to verify whether the conditions in their outer accretion disks are different, as one might expect in case of having accretion triggered by mergers in RL quasars and by secular processes in RQ quasars (Chiaberge et al. 2015), and/or having accretion flows characterized by higher magnetization in the RL quasars as compared with the RQ ones. Obviously, if existing, the largest difference in the  $R$  should be noticed between the RQ quasars and the most RL ones. Hence, unlike in similar studies performed by Ma & Wang (2013), our RQ quasar sample was chosen to be represented only by quasars with FR II radio-morphology. Furthermore, in order to exclude possible differentiating effects coming from different BH masses, Eddington-ratios, and redshifts, we perform such comparison by respective pairings of RL and RQ quasars. First, when deriving dependence of  $R$  on  $\lambda_{\text{E}}$ , we pair each RL quasar

<sup>★</sup> E-mail: mgupta@camk.edu.pl

<sup>†</sup> E-mail: sikora@camk.edu.pl

<sup>‡</sup> E-mail: knalew@camk.edu.pl

with a RQ one with the same redshift and black hole masses. Second, when studying dependence of  $R$  on the black hole mass, we pair quasars with the same redshift and  $\lambda_E$ . Third, when studying dependence of  $R$  on the redshift, we pair quasars with the same  $\lambda_E$  and black hole mass.

Our work is organized as follows: in §2 we define our data samples, in §3 the methods of calculation of  $R$  and pairing procedures are described, in §4 results of our studies of covering factors of dusty obscurers in FR II vs. RQ quasars are presented, and in §5 they are discussed in the context of the radio diversity of quasars. We adopted  $\Lambda$  cold dark matter cosmology, with  $H_0 = 70 \text{ km s}^{-1}$ ,  $\Omega_m = 0.3$  and  $\Omega_\Lambda = 0.7$ .

## 2 DATA SAMPLES

### 2.1 FR II quasars

We compile the sample of RL quasars with FR II radio morphology (Fanaroff & Riley 1974) by cross-matching the sample of FR II radio sources identified by van Velzen et al. (2015) in the Faint Images of the Radio Sky at Twenty-centimeters (FIRST) catalog with the quasars from SDSS DR7 quasar catalog (Schneider et al. 2010). The resulting sample of FR II quasars was then matched with the sample of SDSS DR7 quasars detected by the Wide-field Infrared Survey Explorer (WISE) (Wu et al. 2012). This gave us 895 FR II quasars detected in the MIR band.

### 2.2 Radio-quiet quasars

The RQ sample with MIR data is constructed from the Wu et al. (2012) sample by removing the sample the FR II quasars selected above and those quasars which have FIRST (Becker et al. 1995) and NVSS (Condon et al. 1998) radio detections. We also removed those objects that were outside the FIRST observation region. This gave us 92445 RQ quasars with MIR detections.

### 2.3 Additional sample criteria

As it is stated in §3, we calculate the MID infrared luminosity, using the flux measured in the WISE/W3 window ( $\lambda \approx 12 \mu\text{m}$ ). In order to avoid having this window too close to the short-wavelength edge of the MIR band in the quasar rest frame, we limit our samples to  $z < 2$ . We also introduce a limit on black hole masses, taking only quasars with  $M_{\text{BH}} > 10^8 M_\odot$ . This is in order to avoid Seyfert galaxies, in which the MIR flux can have a significant contribution from starbursts. Furthermore, putting limits on redshift and black hole mass reduces biases imposed on studied properties by selection effects related to the flux limits. Finally, we constrain our samples to the objects with the Eddington-ratio  $\lambda_E > 0.01$  to assure that accretion flows in the selected objects are radiatively efficient. After applying all these limits we end-up with 797 FR II quasars and 67480 RQ quasars.

In Figure 1 we show the histograms of our RL and RQ samples as a function of redshift  $z$ , black hole mass  $M_{\text{BH}}/M_\odot$ , and Eddington ratio  $\lambda_E$ .

## 3 METHODS

### 3.1 Covering factor

There are two main methods to derive covering factors of dusty, circumnuclear obscurers, using number ratio of type 1 to type 2 AGNs

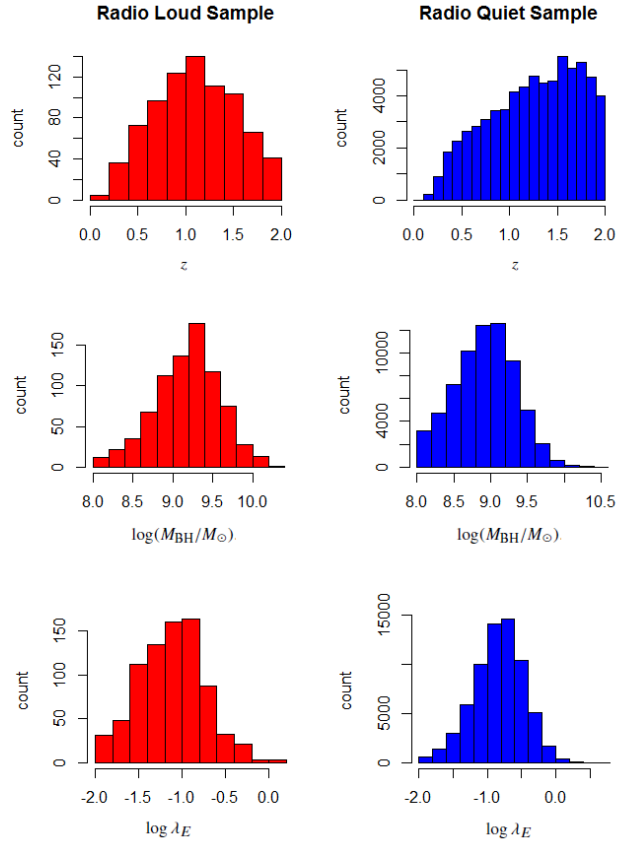


**Figure 1.** Distributions of our RL and RQ samples of quasars in redshift  $z$ , black hole mass  $M_{\text{BH}}/M_\odot$ , and Eddington ratio  $\lambda_E = L_{\text{bol}}/L_{\text{Edd}}$ .

or using ratio of the MIR luminosity to the bolometric luminosity (see review by Netzer 2015). Both methods suffer from several drawbacks, the former because of difficulties to assure the common parent AGN population and because of having dependence of  $N_2/N_1$  on the covering factor distributions (Ramos Almeida et al. 2011; Elitzur 2012), the latter because derivation of the covering factor from  $L_{\text{MIR}}/L_{\text{bol}}$  requires knowledge of anisotropy of accretion disk and obscurer radiation, and those are model dependent. In this paper we will assume that the covering factor is simply equal to  $R \equiv L_{\text{MIR}}/L_{\text{bol}}$ , which corresponds with assumption of isotropic radiation of both components. While quantitatively this may lead to large systematic departures from real values of covering factors (see, e.g. Calderone et al. 2012), as long as our main interest is to verify whether dusty obscurers in RL and RQ quasars are different, using  $R$  is not expected to affect studied by us trends. We calculate  $R$  taking  $L_{\text{bol}}$  from Shen et al. (2011) and  $L_{\text{MIR}}$  using formula  $L_{\text{MIR}} = 12.5 \times (\nu_{\text{W3}} L_{\nu, \text{W3}})$ , where  $\nu_{\text{W3}} = 10^{13.4} \text{ Hz}$ ,  $L_{\nu, \text{W3}} = 4\pi d_L^2 F_{\nu, \text{W3}}$ ,  $\log F_{\nu, \text{W3}} = -(5.174 + m_{\text{W3}})/2.5$ , and  $m_{\text{W3}}$  magnitudes are provided by Wu et al. (2012), denoted in Table 1 as ‘W3’.

Our choice of using WISE/W3 data to calculate  $L_{\text{MIR}}$  can be justified by noting that:

- circumnuclear dust spectra in the AGN rest frames are approximately flat, i.e., with a spectral index  $\alpha_{\text{MIR}} \approx 1$  ( $\alpha : F_\nu \propto \nu^{-\alpha_{\text{MIR}}}$ ) and enclosed between  $2 \mu\text{m}$  and  $25 \mu\text{m}$  (Hönig et al. 2011; Netzer 2015);

**Table 1.** Center wavelengths and frequencies of the four WISE bands. The fourth column gives  $\Delta m$  which is used to transform the the given Vega magnitudes to the AB magnitude system.

Band	$\lambda(\mu m)$	$\log(\nu)$ (Hz)	$\Delta m$
1	3.435	13.94	2.699
2	4.6	13.81	3.339
3	11.56	13.41	5.174
4	22.08	13.13	6.620

- for redshifts  $z > 1.3$  the W1 and W2 bands move in the quasar rest frame to  $\lambda_E < 2\mu m$ ;
- W4 fluxes have much larger S/N than in other channels, hence calculating  $L_{MIR}$  by using spectral slopes between separated by less than factor two  $\nu_{W2}$  and  $\nu_{W3}$  may create much larger errors than using only W3 flux and adopting  $\alpha_{MIR} = 1$ .

### 3.2 Pair Matching

We use a matching technique used in Kauffmann et al. (2008), Masters et al. (2010) and Wild et al. (2010) instead of globally comparing the properties of the RL and RQ samples with different distributions of black hole mass or redshift. In order to study the dependence of  $R$  on any of the three parameters  $\lambda_E$ ,  $M_{BH}$  or  $z$ , each RL quasar is associated with the same number  $n$  of RQ quasars according to their matching distance calculated for the other two parameters. First, candidate RQ counterparts are selected from the following range:  $|\Delta \log \lambda_E| < 0.09$ ,  $|\Delta z| < 0.01$  and  $|\Delta \log M_{BH}| < 0.12$ . Second, we calculate the matching distances between the RL quasar and the RQ candidates defined as  $d_{match}^2 = \sum_i \Delta_i^2$ , where  $\Delta_i$  stands for either  $\Delta \log \lambda_E$ ,  $\Delta z$  or  $\Delta \log(M_{BH}/M_\odot)$ . Then, we select only those RQ candidates which have the shortest matching distance  $d_{match}$ . We have considered different numbers of paired RQ quasars with  $n = 1, 3, 10$ . This process of matching can result in the same RQ quasar paired with more than one RL ones.

Then, the sample of RL quasars, and the subsample of paired RQ quasars, are divided according to the studied parameter into several bins containing equal numbers of sources. For example, in order to study the dependence of  $R$  on  $\lambda_E$ , we divide the samples in the bins of  $\lambda_E$ , and then we pair the quasars in  $M_{BH}$  and  $z$  according to the matching distance given by  $d_{match}^2 = (\Delta z)^2 + [\Delta \log(M_{BH}/M_\odot)]^2$ .

## 4 RESULTS

Figure 2 compares the overall normalized distributions of  $R$  for RL and RQ quasars that are paired in  $z$ ,  $M_{BH}$  and  $\lambda_E$  with  $n = 3$ . We have overlaid the cumulative distributions of the two samples. The typical values of  $R$  for both RL and RQ quasars are in the range 0.1 – 0.6. The histograms peak at  $R_{peak} \simeq 0.25$ , with  $R_{peak}$  being slightly higher for the RQ quasars. The mean values of  $R$  are 0.28 for RQ quasars and 0.32 for RL quasars, and the median values are 0.25 and 0.29, respectively.

In Figure 3 and Figure 4 we show the distributions of  $R$  vs. either  $\lambda_E$ ,  $M_{BH}$  or  $z$  for the paired samples of RL and RQ quasars. Table 2 reports the median values  $R_{50}$ , as well as first and third quartiles  $R_{25}$  and  $R_{75}$  for different bins of  $\lambda_E$ , corresponding to the left panel of Figure 3. There is no overall trend that we see in the distribution of  $R$ . The difference in  $R$  between RL and RQ increases with

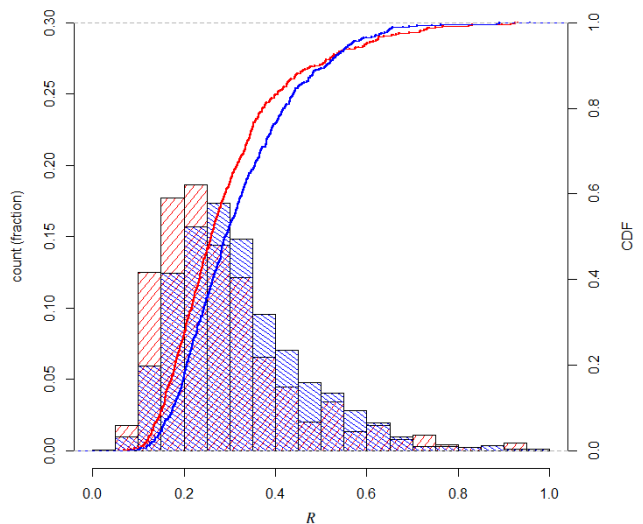


**Figure 2.** Normalised and cumulative distributions of dust covering factor  $R$  for our RL sample (red) and the RQ subsample paired with  $n = 3$  (blue).

**Table 2.** Tabulated results of the sample matched on  $z$  and  $M_{BH}$ . We show the median value of  $\lambda_E$  for each of the bins, the numbers of sources  $N$ , the median value of  $R$ , the standard deviation of  $R$  distribution  $\sigma_R$ , and the 25<sup>th</sup> and 75<sup>th</sup> percentiles of  $R$ .

$\log \lambda_{E,50}$	class	$N$	$R_{50}$	$\sigma_R$	$R_{25}$	$R_{75}$
-1.695	RL	86	0.282	0.177	0.178	0.418
-1.71	RQ	233	0.291	0.170	0.221	0.427
-1.45	RL	89	0.289	0.164	0.192	0.391
-1.46	RQ	249	0.301	0.142	0.234	0.419
-1.31	RL	95	0.256	0.140	0.206	0.340
-1.3	RQ	271	0.307	0.155	0.226	0.392
-1.17	RL	88	0.264	0.132	0.199	0.343
-1.15	RQ	253	0.288	0.136	0.204	0.385
-1.04	RL	92	0.236	0.148	0.171	0.336
-1.04	RQ	261	0.284	0.127	0.198	0.371
-0.93	RL	101	0.242	0.116	0.178	0.308
-0.93	RQ	301	0.273	0.143	0.212	0.357
-0.8	RL	98	0.264	0.131	0.191	0.341
-0.79	RQ	290	0.293	0.121	0.234	0.379
-0.54	RL	93	0.211	0.122	0.160	0.268
-0.53	RQ	282	0.304	0.114	0.229	0.373

the increase in  $\lambda_E$ ,  $z$ , and  $M_{BH}$ . This trend remains the same, irrespective of the number of matches being  $n = 1, 3, 10$ , and whether the bins are equally spaced or contain equal number of objects. We also observe that  $R_{25}$  and  $R_{75}$  indicate broad distributions of  $R$  for every  $\lambda_E$ ,  $M_{BH}$  and  $z$ . Therefore, variations in the median values do not appear to be significant.

Figure 5 shows the cumulative distributions of  $R$  for the samples shown in Figure 3 divided according to  $\lambda_E$  into bins containing equal number of objects. In order to evaluate whether there are statistical differences between the distributions of  $R$  for RL and RQ samples, we make use of the two-sample Kolmogorov-Smirnov test (K-S test). Table 3 shows the  $D$ -values and  $p$ -values of each bin. For a broad range of  $\lambda_E$  values, the values of  $p$  range between 0.001 and 0.15, indicating that the difference between the distributions of  $R$  are not very significant. However, for the highest values

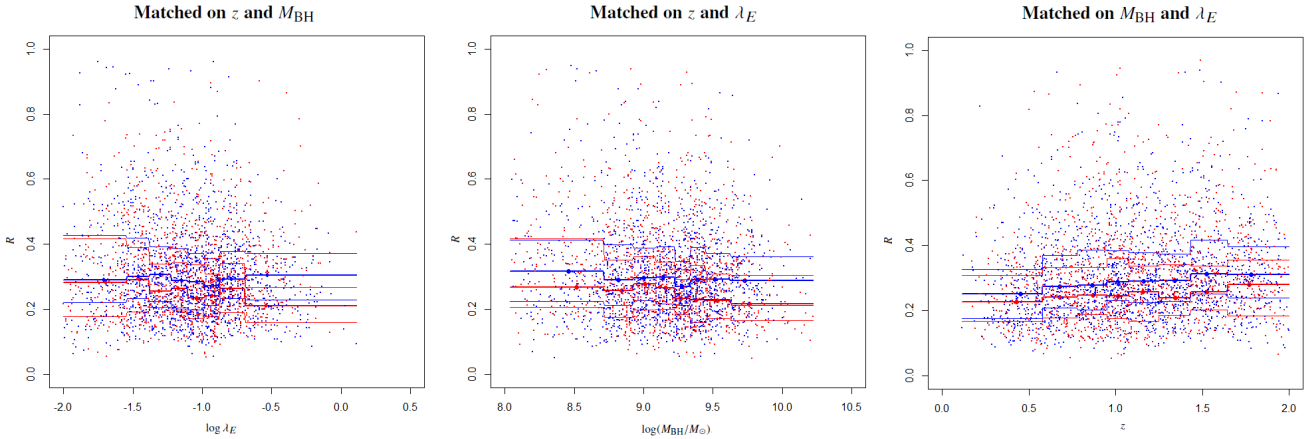


**Figure 3.** Dependence of  $R$  on Eddington ratio  $\lambda_E$  shown in the *left panel*, black hole mass  $M_{\text{BH}}$  shown in the *middle panel* and redshift  $z$  as shown in the *panel to the right panel*. The *red points* represent the RL sample, while *blue points* represent the RQ subsample paired with  $n = 3$ . The *thick lines* show the median value for bins containing equal numbers of sources. The *thin lines* represent the 25<sup>th</sup> and 75<sup>th</sup> percentiles of the respective data.

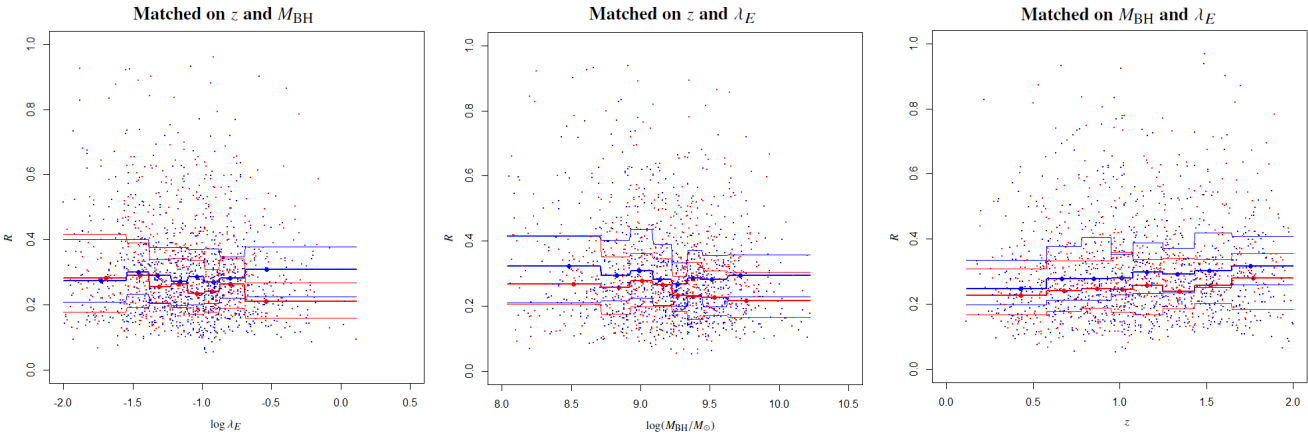


**Figure 4.** Same as Figure 3, but for  $n = 1$ .

**Table 3.** Results of the Kolmogorov-Smirnov test applied to the distribution in  $R$  of RL and paired RQ quasars binned according to the Eddington ratio  $\lambda_E$ .

$\log \lambda_E$	$D$	$p$
[-2.00, -1.55]	0.157	0.096
[-1.54, -1.39]	0.176	0.035
[-1.38, -1.23]	0.193	0.011
[-1.22, -1.11]	0.141	0.150
[-1.10, -0.99]	0.174	0.033
[-0.98, -0.88]	0.218	0.001
[-0.87, -0.70]	0.148	0.082
[-0.69, 0.11]	0.398	$4.67 \times 10^{-10}$

of  $\log \lambda_E \in [-0.69 : 0.11]$ , we obtain  $p < 10^{-9}$ , which indicates significant discrepancy, with the RL quasars having median covering factors lower by  $\Delta R = 0.094$ .

## 5 DISCUSSION AND CONCLUSIONS

While the main factor determining the radiative efficiency of accretion flows in AGN is the accretion rate normalized by the black hole mass (equivalently, the accretion-rate Eddington ratio  $\dot{M}c^2/L_E$ ), the efficiency of jet production covers 3-4 orders of magnitude at any Eddington ratio (Sikora et al. 2007). This is particularly well documented in the case of quasars, in which radio-loudness, defined to be the radio-to-optical luminosity ratio (Kellermann et al. 1989), can be monitored down to lowest values of radio luminosity associated with jet activity. (Kimball et al. 2011). However like in X-ray BH binaries the AGN jet activity is common only at low-rate, radiatively inefficient accretion flows. At larger accretion rates, the jet production is typically very suppressed. This is evidenced by having only  $\sim 10\%$  of quasars associated with radio sources powered by jets, and only about 2% developing luminous, extended FR II radio structures (White et al. 2007). In order to explain the existence of RL quasars and their rarity, one might consider an intermittency of jet production at high accretion rates and its low duty cycle. Such intermittency have been proposed to be driven by stochastic switches between two accretion modes, one driven by viscosity and another led by removing angular momen-

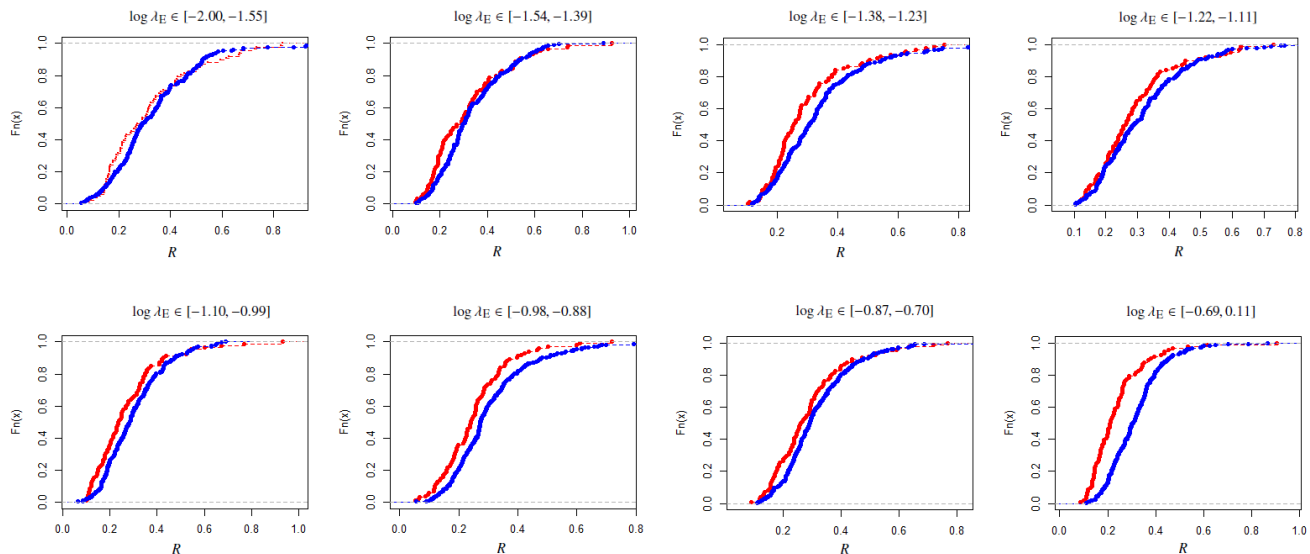


**Figure 5.** Cumulative distributions of  $R$  for the subsamples of RL quasars (red) and RQ quasars (blue) paired with  $n = 3$  for several bins of the Eddington ratio  $\lambda_E$  containing equal number of sources.

tum via MHD outflows (Livio et al. 2003; K rding et al. 2006). However, noting the  $10^7 - 10^8$ -year lifetimes of FR II radio sources (Bird et al. 2008; Antognini et al. 2012, and refs. therein), the rarity of FR II quasars might imply that the RQ quasar lifetimes are longer than the Salpeter timescale (Salpeter 1964). Furthermore, spectral properties of RQ and RL quasars are strikingly similar in all bands but radio (Sanders et al. 1989; Francis et al. 1993; Elvis et al. 1994; Zheng et al. 1997; Telfer et al. 2002; Richards et al. 2006; de Vries et al. 2006; Shang et al. 2011; Shankar et al. 2016). This suggests that production of powerful jets may not be related to some exceptional accretion mode, and seems to favor powering of jets by rotating black holes (Blandford & Znajek 1977). In such a case, the jet power scales roughly with the square of the BH spin and magnetic flux threading the BH horizon  $L_j \propto a^2 \Phi_{\text{BH}}$ . While value of the spin  $a$  is largely determined by cosmological evolution of BHs that involves multiple accretion and merger events (Volonteri et al. 2013), the magnetic flux  $\Phi_{\text{BH}}$  is built up on black hole by advection of a poloidal magnetic field. If accumulation of the magnetic flux proceeds during the quasar phase, one might expect weaker magnetization of the accretion flows in RQ quasars than in RL quasars. Since the magnetization level of accretion flow may affect the covering factor of dusty obscurer (e.g., when obscuration is provided by magnetized winds), such magnetic differentiation of accretion flows in their outermost portions can be verified by studies of a fraction of AGN optical/UV radiation reprocessed by dust to IR radiation.

Until now, most studies of dust covering factor were performed separately for RL and RQ quasars, and focused on their dependence on luminosity, rather than on Eddington ratio. The only work to our knowledge which provides direct comparison of covering factors in RL and RQ quasars, and their dependence on Eddington ratio and BH mass, is the one by Ma & Wang (2013). No significant differences of these properties between the two quasar populations have been found. We performed a similar study, but in order to have a larger radio-loudness contrast between the RL and RQ samples, we limited the RL quasar sample only to those associated with FR II morphology that are known to be on average much

radio-louder than the entire, radio detected population of quasars (Lu et al. 2007). Furthermore, in order to avoid the potential effect of different black hole masses and source distances on the studied properties of RL vs. RQ quasars, we compared their covering factors by including only those RQ quasars, that match the RL ones in redshift, black hole mass and Eddington ratio.

Our main results can be summarized as follows:

- Median covering factors (proxied by  $R$ ) of FR II quasars and RQ quasars matched in ( $z$ ;  $M_{\text{BH}}$ ;  $\lambda_E$ ) are comparable ( $R_{50,\text{RL}} = 0.28$  and  $R_{50,\text{RQ}} = 0.31$ ), both having very similar, fully overlapped broad distributions;
- Dependencies of the median covering factors on the Eddington ratio, black hole mass and redshift are statistically weak. While very similar at lowest values of  $z$ ,  $M_{\text{BH}}$  and  $\lambda_E$ , they diverge somewhat at the highest values of these parameters, with a trend of the median of  $R_{\text{RL}}$  decreasing with both  $\lambda_E$  and  $M_{\text{BH}}$ , and the median of  $R_{\text{RQ}}$  increasing with redshift.

Very similar covering factors of dusty obscurers in FR II and RQ quasars suggest similar accretion conditions on parsec scales. Furthermore, the lack of statistically significant dependence of CFs on the Eddington ratio down to values  $\lambda_E < 0.03$  (found also by Ma & Wang 2013) excludes the possibility that dusty obscurers could be associated with the winds powered by radiation pressure exerted on dust. On the other hand, recent interferometric MIR observations (L pez-Gonzaga et al. 2016) indicate possible elongation of the dusty obscurers in the direction corresponding to the AGN polar axis (as determined by OIII line cones and/or jets), rather than in the equatorial plane. This would indicate outflows/winds as the loci of dust reprocessing AGN radiation into MIR. Such outflows might be powered magnetically as suggested by Emmering et al. (1992), K nigl & Kartje (1994) and Elitzur & Shlosman (2006). The elongated geometry of dusty obscurers is also supported by the fact that scattering cones in quasars are much narrower than predicted by torus models (Obied et al. 2016). Significant magnetization of the accretion flows is independently supported by the fact that

contribution of magnetic fields to vertical pressure in accretion disks can protect them against their gravitational fragmentation (Begelman & Pringle 2007; Salvesen et al. 2016). However, similar covering factors of dusty obscurers in RQ and RL quasars indicate that magnetization of accretion flows in RL quasars is not stronger than in RQ quasars. We can envisage two scenarios for reconciling this similarity with models involving the Blandford-Znajek mechanism, according to which efficiency of jet production strongly depends on the magnetic flux. They are: (1) accumulation of the magnetic flux prior to the quasar phase, which may depend strongly on the environment conditions (Sikora et al. 2013; Sikora & Begelman 2013); (2) magnetic flux accumulation during the quasar phase, in which case the amount of accumulated flux can on average be much larger in RL quasars if their lifetime is much longer than the lifetime of RQ quasars (Schawinski et al. 2015). Obviously, noting that only few nearby AGNs were imaged by MIR interferometry, it remains uncertain how representative are these objects for the entire AGN population. Noting the ambiguity of models that can successfully reproduce the observed IR spectra (Netzer 2015), better understanding of the dusty obscurer structure will need to wait for the next generation of the MIR interferometers (e.g. Lopez et al. 2014).

## ACKNOWLEDGEMENTS

We acknowledge financial support by the Polish NCN grant 2013/09/B/ST9/00026.

## REFERENCES

- Antognini, J., Bird, J., & Martini, P. 2012, *ApJ*, 756, 116
- Antonucci, R. R. J., & Miller, J. S. 1985, *ApJ*, 297, 621
- Barthel, P. D. 1989, *ApJ*, 336, 606
- Barvainis, R. 1987, *ApJ*, 320, 537
- Becker, R. H., White, R. L., & Helfand, D. J. 1995, *ApJ*, 450, 559
- Begelman, M. C., & Pringle, J. E. 2007, *MNRAS*, 375, 1070
- Bird, J., Martini, P., & Kaiser, C. 2008, *ApJ*, 676, 147
- Blandford, R. D., & Znajek, R. L. 1977, *MNRAS*, 179, 433
- Burtscher, L., Meisenheimer, K., Tristram, K. R. W., et al. 2013, *A&A*, 558, A149
- Calderone, G., Sbarrato, T., & Ghisellini, G. 2012, *MNRAS*, 425, L41
- Chiaberge, M., Gilli, R., Lotz, J. M., & Norman, C. 2015, *ApJ*, 806, 147
- Condon, J. J., Cotton, W. D., Greisen, E. W., et al. 1998, *AJ*, 115, 1693
- de Vries, W. H., Becker, R. H., & White, R. L. 2006, *AJ*, 131, 666
- Edelson, R. A., Malkan, M. A., & Rieke, G. H. 1987, *ApJ*, 321, 233
- Elitzur, M. 2012, *ApJ*, 747, L33
- Elitzur, M., & Shlosman, I. 2006, *ApJ*, 648, L101
- Elvis, M., Wilkes, B. J., McDowell, J. C., et al. 1994, *ApJS*, 95, 1
- Emmering, R. T., Blandford, R. D., & Shlosman, I. 1992, *ApJ*, 385, 460
- Fanaroff, B. L., & Riley, J. M. 1974, *MNRAS*, 167, 31P
- Francis, P. J., Hooper, E. J., & Impey, C. D. 1993, *AJ*, 106, 417
- Hönig, S. F., Leipski, C., Antonucci, R., & Haas, M. 2011, *ApJ*, 736, 26
- Hopkins, P. F., Hayward, C. C., Narayanan, D., & Hernquist, L. 2012, *MNRAS*, 420, 320
- Kauffmann G., Heckman T. M., Best P. N., 2008, *MNRAS* 384, 953
- Kellermann, K. I., Sramek, R., Schmidt, M., Shaffer, D. B., & Green, R. 1989, *AJ*, 98, 1195
- Kimball, A. E., Kellermann, K. I., Condon, J. J., Ivezić, Ž., & Perley, R. A. 2011, *ApJ*, 739, L29
- Kishimoto, M., Hönig, S. F., Antonucci, R., et al. 2012, *Journal of Physics Conference Series*, 372, 012033
- Konigl, A., & Kartje, J. F. 1994, *ApJ*, 434, 446
- Koshida, S., Minezaki, T., Yoshii, Y., et al. 2014, *ApJ*, 788, 159
- Körding, E. G., Jester, S., & Fender, R. 2006, *MNRAS*, 372, 1366
- Krolik, J. H., & Begelman, M. C. 1988, *ApJ*, 329, 702
- Lawrence, A., & Elvis, M. 2010, *ApJ*, 714, 561
- Lopez, B., Lagarde, S., Jaffe, W., et al. 2014, *The Messenger*, 157, 5
- López-Gonzaga, N., Burtscher, L., Tristram, K. R. W., Meisenheimer, K., & Schartmann, M. 2016, arXiv:1602.05592
- Livio, M., Pringle, J. E., & King, A. R. 2003, *ApJ*, 593, 184
- Lu, Y., Wang, T., Zhou, H., & Wu, J. 2007, *AJ*, 133, 1615
- Ma, X.-C., & Wang, T.-G. 2013, *MNRAS*, 430, 3445
- Masters K. L., et al., 2010, *MNRAS*, 405, 783
- Miley, G. K., Neugebauer, G., & Soifer, B. T. 1985, *ApJ*, 293, L11
- Miller, J. S., & Goodrich, B. F. 1987, *BAAS*, 19, 695
- Netzer, H. 2015, *ARA&A*, 53, 365
- Netzer, H., Lani, C., Nordon, R., et al. 2015, arXiv:1511.07876
- Obied, G., Zakamska, N. L., Wylezalek, D., & Liu, G. 2016, *MNRAS*, 456, 2861
- Ramos Almeida, C., Levenson, N. A., Alonso-Herrero, A., et al. 2011, *ApJ*, 731, 92
- Rees, M. J., Silk, J. I., Werner, M. W., & Wickramasinghe, N. C. 1969, *Nature*, 223, 788
- Reyes, R., Zakamska, N. L., Strauss, M. A., et al. 2008, *AJ*, 136, 2373
- Richards, G. T., et al., 2006, *ApJS*, 166, 470
- Richards, G. T., Lacy, M., Storrie-Lombardi, L. J., et al. 2006, *ApJS*, 166, 470
- Salpeter, E. E. 1964, *ApJ*, 140, 796
- Salvesen, G., Armitage, P. J., Simon, J. B., & Begelman, M. C. 2016, arXiv:1602.04810
- Sanders, D. B., Phinney, E. S., Neugebauer, G., Soifer, B. T., & Matthews, K. 1989, *ApJ*, 347, 29
- Schawinski, K., Koss, M., Berney, S., & Sartori, L. F. 2015, *MNRAS*, 451, 2517
- Schneider, D. P., Richards, G. T., Hall, P. B., et al. 2010, *AJ*, 139, 2360
- Shang, Z., Brotherton, M. S., Wills, B. J., et al. 2011, *ApJS*, 196, 2
- Shankar, F., Calderone, G., Knigge, C., et al. 2016, *ApJ*, 818, L1
- Shen, Y., Richards, G. T., Strauss, M. A., et al. 2011, *ApJS*, 194, 45
- Sikora, M., Stawarz, Ł., & Lasota, J.-P. 2007, *ApJ*, 658, 815
- Sikora, M., & Begelman, M. C. 2013, *ApJ*, 764, L24
- Sikora, M., Stasińska, G., Koziel-Wierzbowska, D., Madejski, G. M., & Asari, N. V. 2013, *ApJ*, 765, 62
- Telfer, R. C., Zheng, W., Kriss, G. A., & Davidsen, A. F. 2002, *ApJ*, 565, 773
- van Velzen, S., Falcke, H., Körding, E. 2015, *MNRAS*, 446, 2985
- Volonteri, M., Sikora, M., Lasota, J.-P., & Merloni, A. 2013, *ApJ*, 775, 94
- White, R. L., Helfand, D. J., Becker, R. H., Glikman, E., & de Vries, W. 2007, *ApJ*, 654, 99
- Wild V., Heckman T., Charlot S., 2010, *MNRAS*, 405, 933
- Wu, X.-B., Hao, G., Jia, Z., Zhang, Y., & Peng, N. 2012, *AJ*, 144, 49
- Zheng, W., Kriss, G. A., Telfer, R. C., Grimes, J. P., & Davidsen, A. F. 1997, *ApJ*, 475, 469

This paper has been typeset from a  $\text{\LaTeX}$  file prepared by the author.